

## A Hybrid Approach on Metamaterial-Loaded Fractal Antenna Design

**D. Prabhakar<sup>1</sup>, C. H. Rajendra Babu<sup>2</sup>, V. Adinarayana<sup>3</sup>, and V. V. K. D. V. Prasad<sup>1</sup>**

<sup>1</sup> Department of ECE, Gudlavalleru Engineering College (A)  
Seshadri Rao Knowledge Village, Gudlavalleru, Andhra Pradesh, India  
prabhakar.dudla@gmail.com, varaprasadvkd@gmail.com

<sup>2</sup> Department of CSE, Andhra Layola Institute of Engineering and Technology, Andhra Pradesh, India  
chikkalarajendra@gmail.com

<sup>3</sup> Department of ECE, Avanthi Institute of Engineering & Technology (AIET), Andhra Pradesh, India  
joy.adi2011@gmail.com

**Abstract** – The paper provides the interoperable hybrid Grasshopper–Grey Wolf optimization (GHGWO) of the Square Split-Ring Resonator (SRR) metamaterial unit cell. This paper discusses the complex phase strategies of the electric and magnetic interplay of the charged microstrip line of the split ring resonator (SRR). Optimized unit of metamaterial cells for their bandwidth enhancement is packed into a new square fractal antenna. In the interim period of dual band efficiency, a new design is introduced for a microstrip line-feeding square fractal antenna with a faulty ground composition. In the second stage, a quasi-static SRR model is being used to streamline its structural parameters in an effort to reinforce the bandwidth so that optimized composition resonates at the required intensity area. In the GHGWO hybrid algorithm, SRR unit cell size limitations should be optimized and the convergence actions of the algorithm improved. Certain evolutions termed modified hybrid BF-PSO classical BFO, chaos PSO and IWO are being tested for efficiency of the Hybrid GHGWO algorithm. In the final stage, optimized SRR unit cells are stacked into a square fractal antenna that provides bandwidth output suited to wireless usages with upper and lower band. The prototype square fractal antenna without and with SRR unit cells is efficiently evaluated by trial results.

**Index Terms** – Grasshopper–Grey Wolf Optimisation (GHGWO), metamaterial unit cell, quasi-static SRR model and microstrip line, Split-Ring Resonator (SRR).

### I. INTRODUCTION

An antenna is known as a broadband unless its impedance or configuration varies considerably over about one octave or more [5]. In contemporary wireless transmission networks the miniaturization of antenna

layout focused on fractal geometry is of significant importance [1].

In this study, we are proposing a new model of a three-step square fractal antenna. The bandwidth of the planned fractal antenna is increased by partial ground plane on the reverse side of a substratum. Secondly, we prioritize bandwidth in the built fractal antenna with the use of MTM unit cells with optimized split-ring resonator. A hybrid Grass Hopper [2], and grey wolf optimization [2] (GHGWO) algorithm are used to optimize structural variables in split ring resonant unit cells. However, a disadvantage of these techniques is the extensive amount of CPU times utilized in determining the numerical solution compared to the fully explicit methods for the same selection of values. Thus if we were to write them in matrix form, the coefficient matrix would be penta diagonal. The rest of paper is structured as follows: Section II discusses the brief review of hybrid GHGWO algorithm is proposed, Section III comprises of experimental results, and Section IV gives a brief conclusion.

Bilal Babayigit et al. [3] developed a Taguchi Method (TM) to model a non-side lobe level deletion (SLL) optimization for the CAA (non-uniform circular antenna array). TM, a rigorous design strategy, incorporated the numerical nature of experiments as a signal to noise ratio and orthogonal array devices. Such methods decrease the design parameters rather than complete factor evaluation, thus increased the rate of convergence and produced more precise solutions. TM's high output in achieving reduced SLLs was demonstrated by experimental results.

Although the methods mentioned above often focus on the problem of the fractal antenna design more effectively for various kinds of problems, there exist some obvious shortages when compared with other algorithms.

## II. PROPOSED METHODOLOGY

### A. Fractal antenna functionality

An antenna that utilizes fractal and self-similar layout to improve the perimeter (internal and external) of the equipment that can send data or obtain electromagnetic radiation inside a particular surface area or velocity may be outlined as a fractal antenna. Up to the third cycle, the process is continued, resulting in new fractal geometry as shown in Fig. 1. Two unit cells (MTM) of the metamaterial are placed on both sides of the feed line above the support to increase the bandwidth of the designed antenna for broadband enhancement [4].

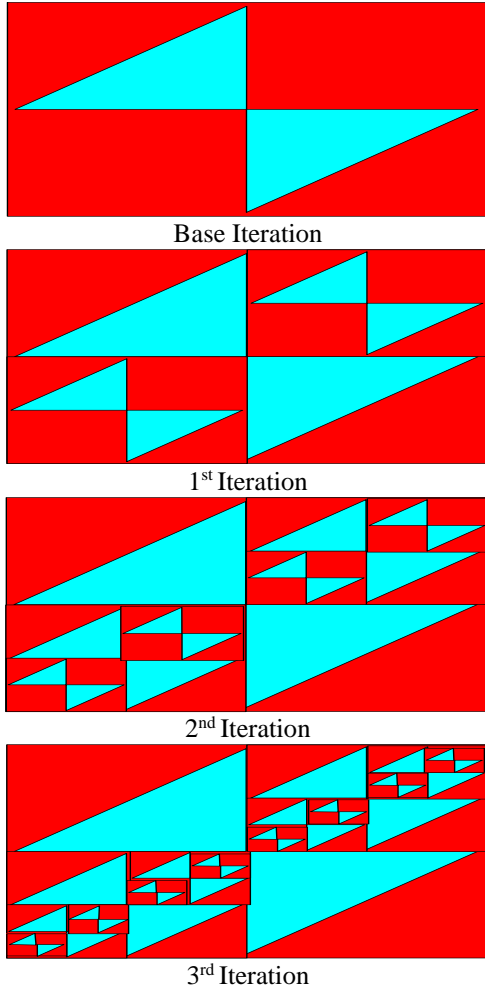


Fig. 1. Proposed square fractal geometry with different iterations (0<sup>th</sup> (base iteration), 1st, 2nd and 3rd).

The model for the proposed fractal antenna is shown in Fig. 2 (a), while Fig. 2 (b) portrays the partial ground layer on the backside of substrate.

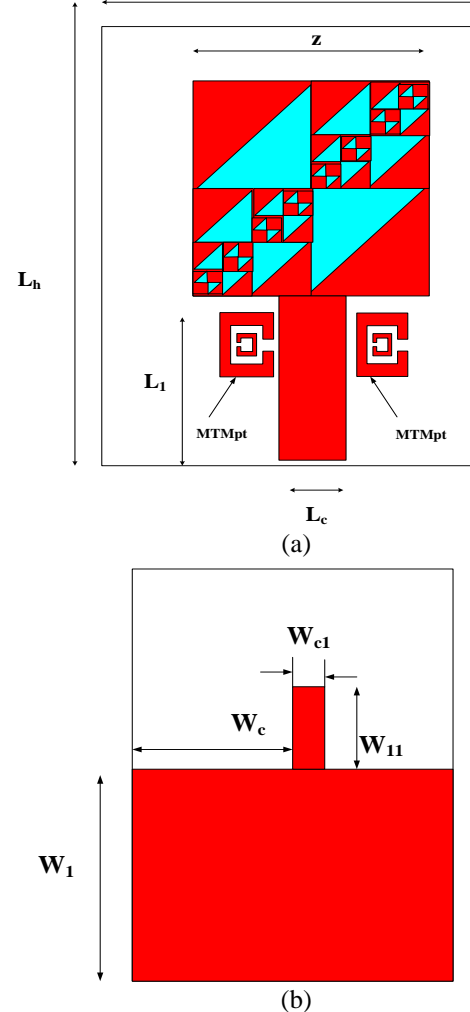


Fig. 2. (a) Top view of optimized fractal antenna. (b) Bottom view of optimized fractal antenna.

### B. Hybridizing GHGWO

Hybridizing Grasshopper (GH) with Grey Wolf Optimization (GWO) to counteract early convergence and long computation time, entangled in large space with local minimums.

The computational modelling used to precisely evaluate the swarming activities of grasshoppers is shown as defines:

$$A_s = C_s + D_s + E_s, \quad (1)$$

where,  $A_s$  Dictates the position of the  $s^{\text{th}}$  grasshopper,  $C_s$  is the social interaction,  $D_s$  is the gravity force and  $E_s$  defines the wind advection.

To provide random behaviour, the equation can be written as  $A_s = rd_1C_s + rd_2D_s + rd_3E_s$ , where  $rd_1$ ,  $rd_2$  and  $rd_3$  are random numbers in  $[0, 1]$ :

$$C_s = \sum_{\substack{v=1 \\ v \neq s}}^p g(e_{sv}) e_{sv}, \quad (2)$$

where,  $e_{sv}$  is the distance between  $s^{\text{th}}$  and the  $v^{\text{th}}$  grasshopper, computed as  $e_{sv} = |d_1 - d_2|$ ,  $g$  is a function to state the strength of social forces, as shown in Eq. (3), and  $e_{sv} = (d_1 - d_2)/e_{sv}$  is a unit vector from the  $s^{\text{th}}$  grasshopper to the  $v^{\text{th}}$  grasshopper.

The  $g$  function, which defines the social forces, is calculated as follows:

$$g(rd) = Pe^{-rd/k} - e^{-rd}, \quad (3)$$

where,  $P$  denotes the intensity of attraction and  $k$  is the length scale. The shape of the function  $g$  have  $D$  component and is computed as:

$$D_s = -qy_q, \quad (4)$$

where,  $q$  is the gravitational constant and  $y_q$  shows a unity vector towards the centre of earth.

The  $E$  component is computed as follows:

$$E_s = kh_b, \quad (5)$$

where,  $k$  is a constant drift and  $h_b$  is a unity vector in wind direction.

The first component of the Eq. (6) will apparently elucidate the location of the present grasshoppers concerning other grasshoppers:

$$P_x^h = z \left( \sum_{\substack{y=1 \\ y \neq s}}^p \frac{u_h - l_h}{2} w(|k_y - k_x|) \frac{k_y - k_x}{h_{xy}} \right) + Q_h. \quad (6)$$

In Eq. (6), the first  $x$  from the left has the same weight as inertial ( $w$ ) in GH. It minimizes grasshopper's movements throughout the goal. Exploration and exploitation of the whole prey balances the parameter. The second  $x$  decreases the attraction zone, comfort zone, and repulsion zone between grasshoppers. By using the element  $z \frac{u_h - l_h}{2} w(|k_y - k_x|)$ ,  $z \frac{u_h - l_h}{2}$  linearly diminishes the space that the grasshoppers should explore and exploit. The element  $w(|k_y - k_x|)$  implies if a grasshopper should be repelled from (exploration) or attracted to (exploitation) the target. The  $z$  internal contributes to a decrease of the repulsion or attraction between grasshoppers proportionally to the number of iterations, and the  $z$  external decreases the search covers around the target with the rise of the iteration count. In short, Eq. (6) first expression, the sum takes into account the role of other grasshoppers and applies the fragility of the grasshopper's relationship [6,7]. The second term  $Q_h$ , facilitates their tendency to travel towards the food source. The parameter  $h$  also facilitates the change in momentum of grasshoppers that evaluate and

subsequently consume the source of food. The coefficient  $c$  minimizes the comfort space in proportion to the number of iterations and computed as defines:

$$h = h_{\max} - a \frac{h_{\max} - h_{\min}}{A}, \quad (7)$$

where,  $h_{\max}$  is the maximum value,  $h_{\min}$  is the minimum value,  $a$  indicates the current iteration, and  $A$  is the maximum number of iterations.

In GHGWO, a search medium upgrades its position by using alpha and beta as shown in Eq. (8):

$$P(t+1) = P + f1 * \text{rand} * ((P_1 - P) + (P_2 - P)) / 2. \quad (8)$$

A further mural for the upgrade of the alpha and beta direction is not upgraded by all people of the population, but by alpha only in the GHGWO proposed to maintain their workforce homogeneity. The proposed algorithm acts as a declining strategy to avoid the local optimum:

$$P(t+1) = P + f1 * \text{rand} * (P_1 - P). \quad (9)$$

Chaos is known for non-linear probabilistic systems as a computational pseudorandom phenomenon. One-dimensional pseudo-invertible maps can produce chaotic motion. This paper uses a well-known chaotic map called a logistic map that depends sensibly on its initial condition. The logistic map is depicted as:

$$P_{t+1} = \mu \cdot P_t (1 - P_t), \quad (10)$$

where,  $P_t$  is a variable, and  $\mu$  is usually set to four, thus for any  $P_t$  located in  $[0, 1]$ , the equation can generate a deterministic chaotic sequences recursively.

A chaotic search strategy was formulated subject to the logistic map. Chaotic search techniques can be interpreted as:

$$P_t^{q+1} = \mu \cdot P_t^q (1 - P_t^q), \quad (11)$$

where,  $P_t^q$  represents the chaotic variable and  $q$  denotes the iteration number.

### C. Split-ring resonator MTM cell configuration

Two concentric conductor circles with divisions in direction opposite to one another comprise of a square split-ring resonator. The magnitudes are much lower than the operational wavelength of these metallic resonant additions and thus, quasi-static theory can be very well implemented in predicting its electromagnetic attitudes using the appropriate RLC resonant model. The integration of SRR with the quasi-static electric system counterpart is shown in Fig. 3 (a) and Fig. 3 (b) represents the equivalent circuit model. The capacitance between the two conductor rings (G12) of the resulting current and voltage distribution is in series in the first half of SRR with a capacitance in the second half of the circle. It is presumed that rings of wavelength "wd" and split length "sl" are the same in both SRR rings for the derivation of the corresponding inductance  $A_d$  and capacitance  $B_d$ . The SRR framework shall be etched

with a thickness of 1.575 mm on a FR4 epoxy substratum. The inductance interpretation  $A_d$  is specified as:

$$A_d = \frac{\mu_0}{2} \frac{h_{avg}}{4} 4.86 \left[ \ln\left(\frac{0.98}{\rho}\right) + 1.84\rho \right], \quad (12)$$

where,  $\mu_0$  is free-space permeability and  $h_{avg}$  is the average strip length of both rings, computed as defies:

$$h_{avg} = 4[rl - (wd + sl)], \quad (13)$$

$rl$  is the length of outer ring,  $wd$  is the width of each ring and  $sl$  is the separation between both rings.

' $\rho$ ' being the filling ratio is given as below:

$$\rho = \frac{wd + sl}{[rl - wd + sl]}. \quad (14)$$

The expression for effective capacitance ' $B_d$ ' is computed as:

$$B_d = \frac{B_{12}}{4} = \left[ rl - \frac{(wd + sl)}{2} \right] B_0, \quad (15)$$

where, ' $B_0$ ' is the per-unit length capacitance between two conductor rings in the presence of dielectric substrate of height ' $ht$ ' and dielectric constant ' $\epsilon_a$ ', presented as follows:

$$B_0 = \epsilon_0 \epsilon_b^t \frac{H(\sqrt{1-m^2})}{H(m)}. \quad (16)$$

Here,  $\epsilon_0$  is free-space permittivity and  $H$  is the complete elliptic integral of first type:

$$m = \frac{sl}{sl + wd}. \quad (17)$$

The  $\epsilon_b^t$ , effective relative permittivity, of dielectric substrate is given as:

$$\epsilon_b^t = 1 + \frac{2}{\pi} \operatorname{arctg} \left[ \frac{ht}{2\pi(wd + sl)} \right] (\epsilon_t - 1). \quad (18)$$

The resonant intensity for the RLC models is generated by  $A_d$  and  $B_d$  (as in Eq. (19)). This is additionally based on geometrical parameters of SRR, i.e., 'rl' outer ring length, 'wd' ring width and 'sl' separation of both rings:

$$f_{q_t} = \frac{1}{2\pi\sqrt{A_d B_d}}. \quad (19)$$

The goal is to optimize SRR layout so that the optimized unit cell resonates at an appropriate resonance frequency by tuning its geometric parameters ( $rl$ ,  $wd$ ,  $sl$ ). Given this goal, the cost function is derived as observes for optimization as:

$$f_{q_{cr}} = f_{q_{dr}} - f_{q_{er}}. \quad (20)$$

The ideal frequency of resonance is ' $f_{q_{dr}}$ ' and the resonant frequency of ' $f_{q_{er}}$ ' is determined using the RLC method. Resonant intensity  $f_{q_t}$  and resonant frequency  $f_{q_{cr}}$  are

related to the built fractal antenna is designed to simulate and observationally tested without metamaterial cells in order to acquire the double band output at 3.68 GHz. When evaluating the data, the signal transmission is interrupted at a 4.4 GHz narrow band which makes the intensity band inoperable.

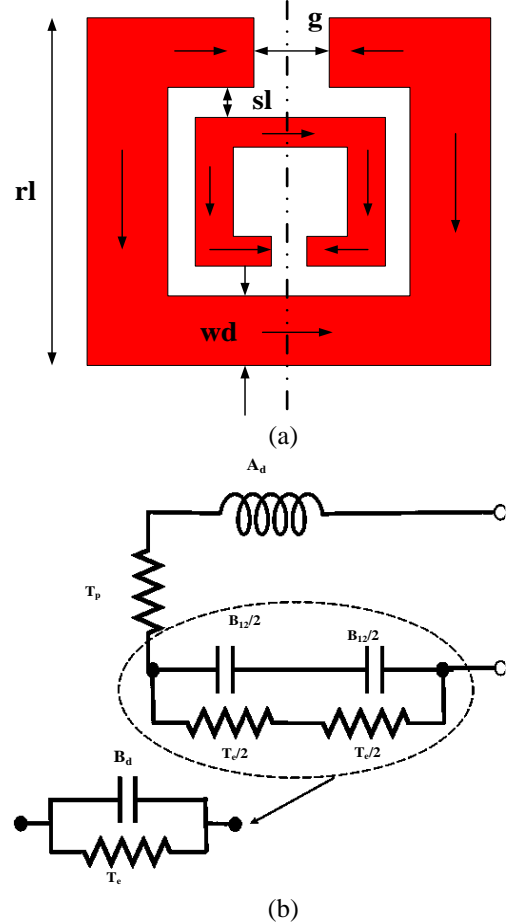


Fig. 3. (a) Structural dimensions of split-ring resonator. (b) Its quasi-debilitated frequency range into usable band, the desired static equivalent circuit model.

#### D. Selection of parameters for optimization algorithms

A wide selection of parameter settings associated with the specific optimization algorithm strongly influences the performance of optimization. For proposed hybrid GHGWO,  $A_s$  Dictates the position of the grasshopper,  $C_s$  is the social interaction,  $D_s$  is the gravity force and  $E_s$  defines the wind advection.

For original BFO techniques and hybrid BF-PSO, highest possible chemical count ' $N_c$ ', reproductive count ' $N_{re}$ ' and removal and neutralization count ' $N_{ed}$ ' are perceived to be 50, 4 and 4, respectively.

### III. EXPERIMENTAL RESULTS

The fitness chart is shown in Fig. 4, the convergence graph. As shown in the graph, the GHGWO, BF-PSO output is close to that of chaos PSO. Nonetheless, the conversion rate is slow compared to other algorithms, while the IWO-classical BFO is compatible with the peak iteration termination requirements.

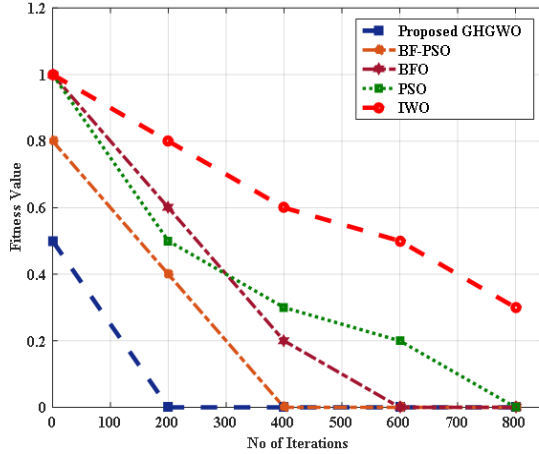


Fig. 4. Convergence plot for proposed GHGWO, modified BF-PSO, classical BFO, PSO and IWO algorithms.

In Table 1 the proposed GHGWO algorithm is obviously efficient in comparison with other algorithms. In this optimizing task, the mean value and standard deviation achieved in the GHGWO algorithm is better than in other algorithms [8, 9]. PSO and modified BF-PSO results are also identical to the GHGWO algorithm:

$$j = \pm \sqrt{\frac{(1+Q_{11})^2 - Q_{21}^2}{(1-Q_{11})^2 - Q_{21}^2}}, \quad (21)$$

$$c^{ik_0 b} = \frac{Q_{21}}{1-Q_{11}} \frac{j-1}{j+1}, \quad (22)$$

$$p = \frac{1}{r_0 b} \left[ \left\{ \left[ \ln \left( c^{ik_0 b} \right) \right]'' + 2w\pi \right\} - s \left[ \ln \left( c^{ik_0 b} \right) \right]' \right], \quad (23)$$

where,  $\left[ \ln \left( c^{ik_0 b} \right) \right]$  represents imaginary components, and

Table 1: Comparative performance of proposed GHGWO algorithm with various methods

Criteria	Proposed GHGWO	Modified BF-PSO	Classical BFO	PSO	IWO
<b>Best solution</b>	0.000001	0.000002	0.000005	0.000002	0.000003
<b>Mean solution</b>	0.054213	0.528061	0.492478	0.517842	0.440051
<b>Worst solution</b>	0.691249	0.741507	0.870005	0.782456	0.880102
<b>Standard deviation</b>	0.354328	0.381412	0.454483	0.418753	0.463854
<b>Average time(T)</b>	4.018	4.546	9.411	4.587	11.151

For optimized antennas loaded with SRR, Fig. 8 shows simulated and measured VSWR performance.

$\left[ \ln \left( c^{ik_0 b} \right) \right]'$  represents real components of complex number  $Q_{11}$  and  $Q_{21}$  are derived correspondingly,  $p$  and  $j$  represent both refractive index and product impedance,  $r_0$  for wave events in free room shows wave number,  $b$  for peak cell length and  $w$  for periodical functions typical of sinusoidal structure. The cell of the MTM unit has a homogenous effective index and impedance, because the optimized size of the external ring ( $rl$ ) is  $\frac{\lambda}{12}$  for the optimal resonant frequency of 4.4 GHz. It makes the simple branch ( $w=0$ ) to be used for continuous refractive index. Active permeability and permeability are extracted from the corresponding refractive index and impedance:

$$\varepsilon = \frac{p}{j}, \quad (24)$$

$$\mu = pj. \quad (25)$$

Figures 5 (a), (b) applies to a Q-parameter ( $Q_{11}$  and  $Q_{21}$ ) magnitude and stage Chart derived from HFSS simulation of optimized SRR design. The real and imaginary portions of derived complex permeability and permittivity are shown in figure 5c d, accordingly. It's evident from the Fig. 5 (c), (d), that in frequency ranges from 3.9 up to 4.5 GHz both permittivity and permeability are negative and hence have dual-negative metamaterial properties in target frequency range. Therefore, the framework used to forecast costs is efficiently using a quasi-static analogous model.

In Fig. 6 displays retarded loss functionality, reflecting an increase of the bandwidth in the newly designed fractal antenna after charging optimized SRR unit cells. From the figure, the fractal antenna contributes to dual-band output at 3.68 GHz and 4.72 GHz without metamaterial unit cells. In the frequency range between 4.2 and 4.5 GHz the signal transmission is limited, so this band felt the impact.

Figure 7 contrasts simulated and measured coefficient outcomes with MTM unit cells, respectively for modelled fractal antenna without charging.

The data are collected from the bench top vector network analyzer with a frequency between 10MHz and 20GHz.

VSWR is an important parameter that indicates a signal feed location corresponding impedance.

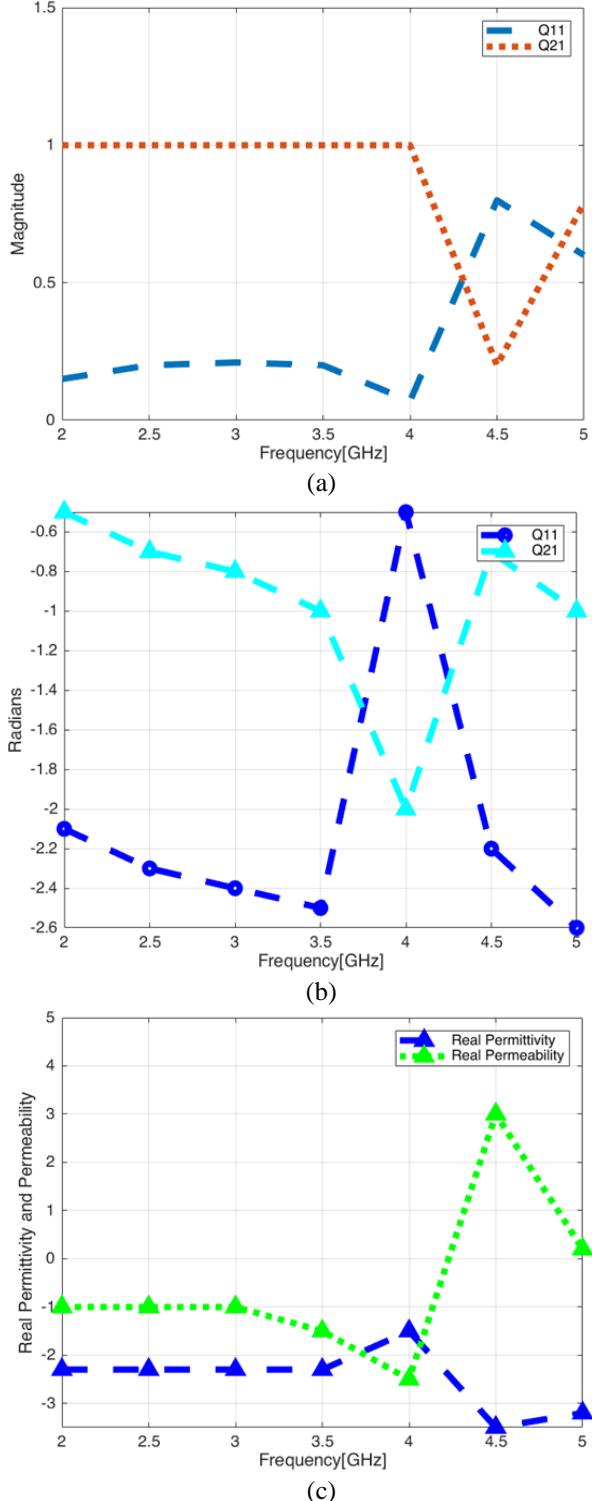


Fig. 5. (a) Extracted magnitude of Q11 and Q21 for optimized SRR. (b) Extracted phase (radians) of Q11 and Q21 for optimized SRR. (c) Real components of permittivity and permeability. (d) Imaginary components of permittivity and permeability.

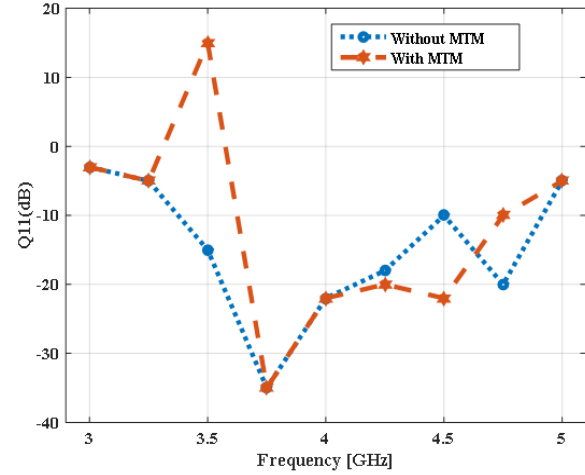


Fig. 6. Antenna without MTM and with MTM performance comparison.

The antenna gain vs. frequency plot for an integrated fractal antenna equipped with SRR shown in Fig. 9. The optimistic strong gain in the small frequency range between 3.44 and 4.85 GHz can be seen. At 4 GHz, the peak frequency is 13.8 dB, and the lowest at 4.4 GHz is 3.2 dB.

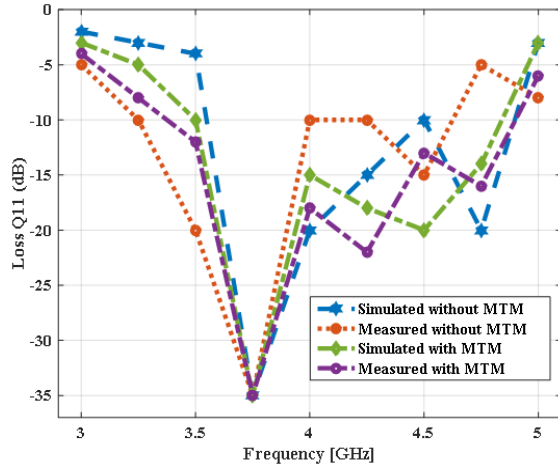


Fig. 7. Return loss properties simulated and measured for fractal antenna cells without and with MTM unit cells.

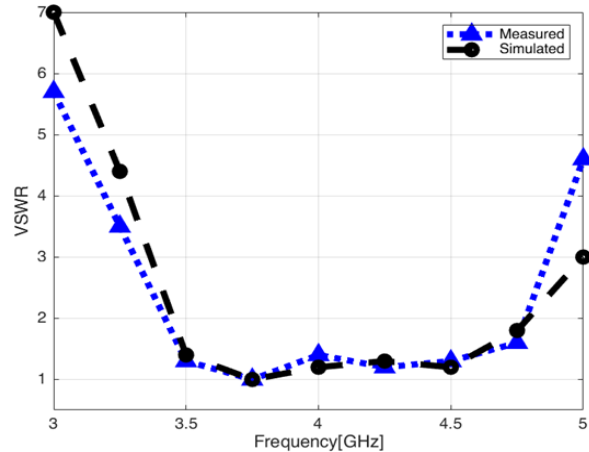


Fig. 8. VSWR for configured SRR-loaded fractal antenna simulated and measured.

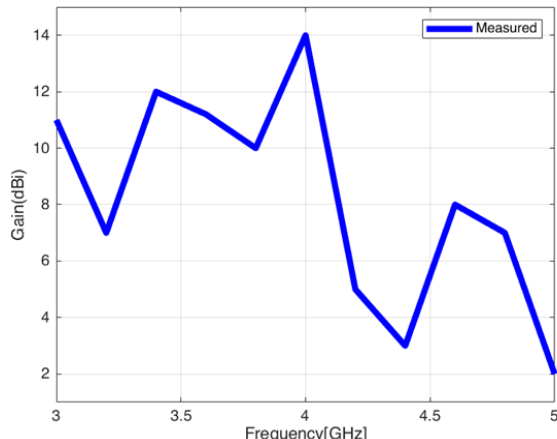


Fig. 9. Measured antenna gain versus frequency track for SRR-presented antennas optimized.

#### IV. CONCLUSION

The paper envisages the new design of a partial-ground square fractal microstrip line-fed antenna. Enhanced rectangular band on a partial plane increases capacitance stability, leading to a double-band output of 3.68 GHz and 4.72 GHz. The GHGWO hybrid algorithm is proven superior to other algorithms due to its stronger mean solution, the lowest standard deviation and substantially lower time. Two square split-ring resonators, a common metamaterial unit cell, are charged after an optimization close to the micro-line feed of the formulated fractal antenna. Upon processing of the antenna with optimized SRR structures, dual band response from the built fractal antenna is converted into bandwidth efficiency (3.49–4.73 GHz). For the conceptual testing of simulation effects the modelled fractal antenna without and with metamaterial mounting is generated. The enhanced findings show that an optimisation in the antenna design and engineering of the SRR metamaterial unit Cell for the throughput progression of the designed fractal antenna.

#### REFERENCES

- [1] D. Werner, R. Haupt, and P. Werner, "Fractal antenna engineering: The theory and design of fractal antenna arrays," *IEEE Antennas and Propagation Magazine*, vol. 41, no. 5, pp. 37-58, 1999.
- [2] E. Ekmekci, K. Topalli, T. Akin, and G. Turhan-Sayan, "A tunable multi-band metamaterial design using micro-split SRR structures," *Optics Express*, vol. 17, no. 18, pp. 16046-16058, 2009.
- [3] D. Srivastava, A. Khanna, and J. Saini, "Design of a wideband gap-coupled modified square fractal antenna," *Journal of Computational Electronics*, vol. 15, no. 1, pp. 239-247, 2015.
- [4] B. Babayigit and E. Senyigit, "Design optimization of circular antenna arrays using Taguchi method," *Neural Computing and Applications*, vol. 28, no. 6, pp. 1443-1452, 2016.
- [5] P. Mishra, S. Pattnaik, and B. Dhaliwal, "Square-shaped fractal antenna under metamaterial loaded condition for bandwidth enhancement," *Progress In Electromagnetics Research C*, vol. 78, pp. 183-192, 2017.
- [6] M. Dorostkar, R. Azim, and M. Islam, "A novel  $\Gamma$ -shape fractal antenna for wideband communications," *Procedia Technology*, vol. 11, pp. 1285-1291, 2013.
- [7] R. Bojanic, V. Milosevic, B. Jokanovic, F. Medina-Mena, and F. Mesa, "Enhanced modelling of split-ring resonators couplings in printed circuits," *IEEE Transactions on Microwave Theory and Techniques*, vol. 62, no. 8, pp. 1605-1615, 2014.

- [8] Y. Choukiker and S. Behera, "Modified Sierpinski square fractal antenna covering ultra-wide band application with band notch characteristics," *IET Microwaves, Antennas & Propagation*, vol. 8, no. 7, pp. 506-512, 2014.
- [9] A. Numan and M. Sharawi, "Extraction of material parameters for metamaterials using a full-wave simulator [Education Column]," *IEEE Antennas and Propagation Magazine*, vol. 55, no. 5, pp. 202-211, 2013.